Research Article | Vol. 8, No. 1 | 1 Jan 2017 | BIOMEDICAL OPTICS EXPRESS 124
Biomedical Optics EXPRESS

Design and characterization of a combined OCT and wide field imaging falloposcope for ovarian cancer detection

MOLLY KEENAN,[1] TYLER H. TATE,[2] KHANH KIEU,[2] JOHN F. BLACK,[3] URS UTZINGER,[1,2] AND JENNIFER K. BARTON[1,2,*]

[1]University of Arizona, Biomedical Engineering, 1127 James E Rogers Way, Tucson, AZ 85721, USA
[2]University of Arizona, College of Optical Sciences, 1630 East University Blvd., Tucson, AZ 85721, USA
[3]Glannaventa Inc., 2276 Allegheny Way, San Mateo, CA 94402, USA
*barton@email.arizona.edu

Abstract: Early detection of ovarian cancer is only achieved in around 20% of women due to lack of effective screening. We propose a method for surveillance of high risk women based on a microendoscope introduced transvaginally to image the fallopian tubes and ovaries. This requires extreme miniaturization of the optics and catheter sheath. We describe the design of a falloposcope that combines optical coherence tomography (OCT) and wide field imaging into a sub-1 mm diameter package. We characterize the systems and show that they provide contrast on *ex-vivo* samples of ovary and fallopian tube. In addition, we show the mechanical performance of the endoscope in an anatomically correct model of the female reproductive tract.

OCIS codes: (170.2150) Endoscopic imaging; (170.3890) Medical optics instrumentation; (170.4500) Optical coherence tomography; (170.4440) ObGyn.

References and links

1. A. Chan, B. Gilks, J. Kwon, and A. V. Tinker, "New Insights Into the Pathogenesis of Ovarian Carcinoma: Time to Rethink Ovarian Cancer Screening," Obstet. Gynecol. **120**(4), 935–940 (2012).
2. R. S. Tuma, "Origin of Ovarian Cancer May Have Implications for Screening," J. Natl. Cancer Inst. **102**(1), 11–13 (2010).
3. Brown P, Palmer C, "The Preclinical Natural History of Serous Ovarian Cancer: Defining the Target for Early Detection" PLOS, **6** (7) (2009).
4. C. P. Crum, R. Drapkin, D. Kindelberger, F. Medeiros, A. Miron, and Y. Lee, "Lessons from BRCA: the tubal fimbria emerges as an origin for pelvic serous cancer," Clin. Med. Res. **5**(1), 35–44 (2007).
5. C. P. Crum, "Intercepting pelvic cancer in the distal fallopian tube: theories and realities," Mol. Oncol. **3**(2), 165–170 (2009).
6. N. Nishida, F. Murakami, and K. Higaki, "Detection of serous precursor lesions in resected fallopian tubes from patients with benign diseases and a relatively low risk for ovarian cancer," Pathol. Int. **66**(6), 337–342 (2016).
7. S. S. Buys, E. Partridge, A. Black, C. C. Johnson, L. Lamerato, C. Isaacs, D. J. Reding, R. T. Greenlee, L. A. Yokochi, B. Kessel, E. D. Crawford, T. R. Church, G. L. Andriole, J. L. Weissfeld, M. N. Fouad, D. Chia, B. O'Brien, L. R. Ragard, J. D. Clapp, J. M. Rathmell, T. L. Riley, P. Hartge, P. F. Pinsky, C. S. Zhu, G. Izmirlian, B. S. Kramer, A. B. Miller, J. L. Xu, P. C. Prorok, J. K. Gohagan, and C. D. Berg; PLCO Project Team, "Effect of screening on ovarian cancer mortality: the Prostate, Lung, Colorectal and Ovarian (PLCO) Cancer Screening Randomized Controlled Trial," JAMA **305**(22), 2295–2303 (2011).
8. S. Vaughan, J. I. Coward, R. C. Bast, Jr., A. Berchuck, J. S. Berek, J. D. Brenton, G. Coukos, C. C. Crum, R. Drapkin, D. Etemadmoghadam, M. Friedlander, H. Gabra, S. B. Kaye, C. J. Lord, E. Lengyel, D. A. Levine, I. A. McNeish, U. Menon, G. B. Mills, K. P. Nephew, A. M. Oza, A. K. Sood, E. A. Stronach, H. Walczak, D. D. Bowtell, and F. R. Balkwill, "Rethinking ovarian cancer: recommendations for improving outcomes," Nat. Rev. Cancer **11**(10), 719–725 (2011).
9. M. A. Brewer, U. Utzinger, J. K. Barton, J. B. Hoying, N. D. Kirkpatrick, W. R. Brands, J. R. Davis, K. Hunt, S. J. Stevens, and A. F. Gmitro, "Imaging of the ovary," Technol. Cancer Res. Treat. **3**(6), 617–627 (2004).
10. M. G. Radvany and R. S. Kiesz, "Plaque Excision in Management of Lower Extremity Peripheral Arterial Disease with the SilverHawk Atherectomy Catheter," Semin. Intervent. Radiol. **25**(1), 11–19 (2008).
11. J. Kerin, E. Surrey, L. Daykhovsky, and W. S. Grundfest, "Development and application of a falloposcope for transvaginal endoscopy of the fallopian tube," J. Laparoendosc. Surg. **1**(1), 47–56 (1990).

#279464 http://dx.doi.org/10.1364/BOE.8.000124
Journal © 2017 Received 26 Oct 2016; revised 2 Dec 2016; accepted 5 Dec 2016; published 8 Dec 2016

Biomedical Optics EXPRESS

12. A. Y. Wong and S. M. Walker, "Falloposcopy--a prerequisite to the proper assessment of tubal infertility," Hong Kong Med. J. **5**(1), 76–81 (1999).
13. D. K. Rex, "Maximizing Detection of Adenomas and Cancers During Colonoscopy," Am. J. Gastroenterol. **101**(12), 2866–2877 (2006).
14. L. P. Hariri, G. T. Bonnema, K. Schmidt, A. M. Winkler, V. Korde, K. D. Hatch, J. R. Davis, M. A. Brewer, and J. K. Barton, "Laparoscopic optical coherence tomography imaging of human ovarian cancer," Gynecol. Oncol. **114**(2), 188–194 (2009).
15. M. Kirillin, O. Panteleeva, E. Yunusova, E. Donchenko, and N. Shakhova, "Criteria for pathology recognition in optical coherence tomography of fallopian tubes," J. Biomed. Opt. **17**(8), 081413 (2012).
16. T. H. Tate, B. Baggett, P. F. Rice, J. W. Koevary, G. V. Orsinger, A. C. Nymeyer, W. A. Welge, K. Saboda, D. J. Roe, K. D. Hatch, S. K. Chambers, U. Utzinger, and J. Barton, "Multispectral fluorescence imaging of human ovarian and fallopian tube tissue for early-stage cancer detection," J. Biomed. Opt. **21**(5), 056005 (2016).
17. J. N. McAlpine, S. El Hallani, S. F. Lam, S. E. Kalloger, M. Luk, D. G. Huntsman, C. MacAulay, C. B. Gilks, D. M. Miller, and P. M. Lane, "Autofluorescence imaging can identify preinvasive or clinically occult lesions in fallopian tube epithelium: a promising step towards screening and early detection," Gynecol. Oncol. **120**(3), 385–392 (2011).
18. T.-Y. Wu, A. R. Rouse, S. K. Chambers, K. D. Hatch, and A. F. Gmitro, "Confocal microlaparoscope for imaging the fallopian tube," J. Biomed. Opt. **19**(11), 116010 (2014).
19. C. M. Lee, C. J. Engelbrecht, T. D. Soper, F. Helmchen, and E. J. Seibel, "Scanning fiber endoscopy with highly flexible, 1 mm catheterscopes for wide-field, full-color imaging," J. Biophotonics **3**(5-6), 385–407 (2010).
20. E. J. Seibel, C. D. Melville, R. S. Johnston, Y. Gong, K. Agnew, S. Chiang, and E. M. Swisher, "In vivo laser-based imaging of the human fallopian tube for future cancer detection," Proc. SPIE **9304**, 93040 (2015).
21. X. Li, C. Chudoba, T. Ko, C. Pitris, and J. G. Fujimoto, "Imaging needle for optical coherence tomography," Opt. Lett. **25**(20), 1520–1522 (2000).
22. D. Lorenser, X. Yang, R. W. Kirk, B. C. Quirk, R. A. McLaughlin, and D. D. Sampson, "Ultrathin side-viewing needle probe for optical coherence tomography," Opt. Lett. **36**(19), 3894–3896 (2011).
23. K. M. Joos and J.-H. Shen, "Miniature real-time intraoperative forward-imaging optical coherence tomography probe," Biomed. Opt. Express **4**(8), 1342–1350 (2013).
24. B. Reimers, D. Nikas, E. Stabile, L. Favero, S. Saccà, A. Cremonesi, and P. Rubino, "Preliminary experience with optical coherence tomography imaging to evaluate carotid artery stents: safety, feasibility and techniques," EuroIntervention **7**(1), 98–105 (2011).
25. D. Kang, R. V. Martinez, G. M. Whitesides, and G. J. Tearney, "Miniature grating for spectrally-encoded endoscopy," Lab Chip **13**(9), 1810–1816 (2013).
26. J. Lee, Y. Chae, Y.-C. Ahn, and S. Moon, "Ultra-thin and flexible endoscopy probe for optical coherence tomography based on stepwise transitional core fiber," Biomed. Opt. Express **6**(5), 1782–1796 (2015).
27. L. Scolaro, D. Lorenser, W.-J. Madore, R. W. Kirk, A. S. Kramer, G. C. Yeoh, N. Godbout, D. D. Sampson, C. Boudoux, and R. A. McLaughlin, "Molecular imaging needles: dual-modality optical coherence tomography and fluorescence imaging of labeled antibodies deep in tissue," Biomed. Opt. Express **6**(5), 1767–1781 (2015).
28. W. Göbel, J. N. D. Kerr, A. Nimmerjahn, and F. Helmchen, "Miniaturized two-photon microscope based on a flexible coherent fiber bundle and a gradient-index lens objective," Opt. Lett. **29**(21), 2521–2523 (2004).
29. H. D. Ford and R. P. Tatam, "Fibre imaging bundles for full-field optical coherence tomography," Meas. Sci. Technol. **18**(9), 2949–2957 (2007).
30. J. Mavadia, J. Xi, Y. Chen, and X. Li, "An all-fiber-optic endoscopy platform for simultaneous OCT and fluorescence imaging," Biomed. Opt. Express **3**(11), 2851–2859 (2012).
31. Y. T. Pan, T. Q. Xie, C. W. Du, S. Bastacky, S. Meyers, and M. L. Zeidel, "Enhancing early bladder cancer detection with fluorescence-guided endoscopic optical coherence tomography," Opt. Lett. **28**(24), 2485–2487 (2003).
32. J. Wu, M. Conry, C. Gu, F. Wang, Z. Yaqoob, and C. Yang, "Paired-angle-rotation scanning optical coherence tomography forward-imaging probe," Opt. Lett. **31**(9), 1265–1267 (2006).
33. E. Lorenzen, F. Follmann, G. Jungersen, and J. S. Agerholm, "A review of the human vs. porcine female genital tract and associated immune system in the perspective of using minipigs as a model of human genital Chlamydia infection," Vet. Res. (Faisalabad) **46**(1), 116 (2015).
34. A. M. Winkler, P. F. S. Rice, R. A. Drezek, and J. K. Barton, "Quantitative tool for rapid disease mapping using optical coherence tomography images of azoxymethane-treated mouse colon," J. Biomed. Opt. **15**(4), 041512 (2010).
35. R. A. McLaughlin, D. Lorenser, and D. D. Sampson, *Handbook of Coherent-Domain Optical Methods* (Springer Science + Business Media, 2013).
36. J. F. Black, T. Tate, M. Keenan, E. Swan, U. Utzinger, and J. Barton, "A six-color four-laser mobile platform for multi-spectral fluorescence imaging endoscopy," Proc. SPIE **9304**, 93040 (2015).
37. M. Keenan, C. Howard, T. Tate, I. McGuiness, A. Sauer-Budge, J. Black, U. Utzinger, and J. K. Barton, "Design of an everting balloon to deploy a microendoscope to the fallopian tubes," Proc. SPIE **9689**, 96890 (2016).

Biomedical Optics EXPRESS

1. Introduction

Ovarian cancer poses a particular challenge for optical imaging due to its deep anatomical location and relative lack of knowledge about its origin and natural history. Recent studies have suggested that what we call ovarian cancer is a complex collection of diseases. One form, high grade serous carcinoma (HGSOC), is the most lethal and responsible for over 70% of ovarian cancer mortality. A growing body of evidence indicates that a significant fraction of this form originates in the distal fallopian tube and migrates to the ovary [1–6]. For cases originating in the fallopian tube, a method that could interrogate the lumen of the fallopian tubes and ovaries at a cellular level, while tumors were less than 0.5 cm, could improve early detection [2,3]. Existing screening methods such as the CA-125 blood test, palpation, and transvaginal ultrasound lack the necessary sensitivity, specificity, and resolution for early diagnosis and may result in false positives [7,8]. Positive indications are followed by further testing, such as laparoscopy, to confirm diagnosis or explore the extent of the disease. Optical methods, which have micron-scale resolution, are non-invasive, can be miniaturized and are particularly well suited for imaging in a conduit [9,10]. Optical fiber-based methods provide the needed flexibility to access a deep site like the ovaries and may provide the same confirmation of diagnosis as laparoscopy while minimizing the use of potentially unnecessary invasive procedures for women with increased risk of developing ovarian cancer.

Falloposcopy was performed *in-vivo* in the early 1990's to investigate blockages as potential reasons for infertility [11,12]. Early falloposcopes used white light delivered through a 0.65 to 1 mm diameter endoscope. Due to the small size requirement, these falloposcopes were limited to a single 3,000 element fiber bundle. To aid introduction into the fallopian tube, the physician used a hysteroscope to access the uterus and visualize the tubal ostium. The lumen was first cannulated with a guide wire before saline irrigation at a pressure of 200 mmHg (0.26 atm, 3.8 psi) [11] was used to open the lumen and facilitate the introduction of the catheter over the guide wire. Once the falloposcope reached the distal end, imaging was performed as the catheter was retracted. While appropriate for the investigation and traversal of macroscopic well-defined blockages, these endoscopes were limited by low resolution and, similar to limitations of white light based colonoscopes, could easily miss small and /or low-intrinsic-contrast suspicious sites [13]. Advances in optical methods, new materials, and construction techniques make it possible to build a new generation of falloposcopes that can better image the tubal mucosa with sensitivity to early stage disease.

Two complementary methods of optical interrogation are used to examine the structural and functional signatures of the fallopian tube. Optical coherence tomography (OCT), an interferometric technique that uses near-infrared light, can image through the lumen surface to around 1-2 mm deep, capturing the microstructural organization in the mucosa and sub-mucosal layers. OCT has been used successfully by our laboratory to distinguish between normal, cancerous, and benign conditions in *ex-vivo* samples of human ovary and fallopian tubes [9]. OCT has also been successfully used laparoscopically for cancer detection for the ovaries [14], as well as to detect cases of pelvic inflammatory disease in the fallopian tubes [15]. Wide field imaging, including multispectral reflectance and autofluorescence [16], can be used for navigation as well as discrimination between normal, benign and cancerous tissues. This method has shown promise for identifying disease in *ex-vivo* human ovary and fallopian tube samples [17]. Autofluorescence imaging utilizes the endogenous fluorophores in the body (e.g. NADH or collagen) to create contrast. Previous studies have also shown that UV excitation at 270 nm, 320 nm and 340 nm may be of particular interest [9]. *In-vivo,* imaging of the fallopian tube lumenal surface has been accomplished in women both from a distal laparoscopic approach using a 2 mm articulating confocal microendoscope [18] and a proximal uterine approach using a 1.2 mm forward viewing white light scanning fiber endoscope [19,20]. Although promising, neither endoscope was able to traverse the entire fallopian tube, suggesting that a smaller, more flexible and steerable endoscope may be necessary to fully interrogate the target.

Biomedical Optics EXPRESS

Recent advances in optics and materials have enabled the development of sub-millimeter endoscopes and needle probes to be used in human studies. The design challenges of these probes lie not only in the limits of miniaturization of optical components but also in achieving large field of view, flexibility, and mechanical stability. Single fiber probes in a rigid rod or needle can be small diameter [21–23], but are limited to either large cavities or tissues that can be safely punctured. Side-viewing, rotational and/or pull-back scanning endoscopes can be small and flexible [24]. Forward-looking endoscopes typically have larger total outer diameter, due to the need to utilize fiber bundles, relatively bulky scanning mechanisms or CMOS detectors. By using a grating to spread light and spectral encoding to maintain resolution, Kang et al., have been able to make durable 500 μm diameter probes [25]. Side-viewing probes designed in this fashion can then be rotated and pulled back to achieve wide field imaging. All fiber, side-viewing OCT probes can be made the same diameter as the optical fiber itself, ~160 μm, although sheath material will add to this diameter [22,25]. The use of a double-clad fiber has enabled simultaneous OCT and point-scanning fluorescence imaging with one 310 μm diameter fiber [27]. For forward viewing systems, solutions include use of a fiber bundle [28], which is appropriate for wide field imaging but remains in the early stages for use with OCT [29], use of piezo scanning mechanisms for use with single fibers [20], or moving optical elements [30]. Depending on the diameter and design of the optical system, a wide field of view is possible. Fiber bundle systems are typically the smallest option but are limited in resolution to the number of core elements. Combined forward-looking fluorescence and OCT endoscopes have been previously utilized but are typically larger than 1 mm in diameter, such as a 4 mm diameter probe for bladder cancer detection [31]. For forward-looking multimodal endoscopes smaller than 1 mm, space is at a premium and passive lens-based imaging is more suitable than electrically actuated moving parts or counter-rotating prisms [32].

The overall objective of this study is to create a sub-millimeter, flexible, steerable endoscope that is capable of wide field imaging (including reflectance and fluorescence) and OCT. Our long-term goal is to detect early stage disease in the fallopian tubes in a point-of-care setting. This endoscope is also a platform for other novel, sub-1 mm diameter highly capable probes. This falloposcope expands on previous work by enabling the lumen of the fallopian tube to be examined from a trans-uterine hysteroscopic-based approach rather than laparoscopically. We discuss the physiological design limits and the optical mechanical design and performance of the falloposcope.

2. General design

The challenges of designing a highly capable microendoscope for the fallopian tubes relate to the mode of access and the tortuosity of the tubes. An instrument needs to pass the cervix via the working channel of a hysteroscope and enter the fallopian tube ostium on the uterine wall. The diameter of the fallopian tube at the ostium is approximately 1 mm and expands to approximately 1 cm at the fimbriae over a length of 12 – 15 cm [33]. At the distal end, part of the fimbrial structure is attached to the ovary, which itself is approximately 4 cm in diameter. Therefore, the falloposcope must be small enough to pass through the ostium but also have a large enough field of view, or be steerable, to image the distal tube and surface of the ovary. The fallopian tube is curved in a patient-specific manner. The lumen of the tube presents another challenge, as it is filled with epithelial folds, mucus, and is typically collapsed on itself, rather than open and fluid-filled like a blood vessel. This means that the entire endoscope must be flexible, the distal end should track in the tube, and the sheath should be smooth, lubricious, and biocompatible. Navigation is essential and therefore the probe should incorporate at least one forward viewing modality with a large field of view to visualize the walls of the tube and opening. Other imaging modalities with higher resolution can be side-viewing in order to better interrogate the potential site of disease, the tubal walls and fimbriae.

Biomedical Optics EXPRESS

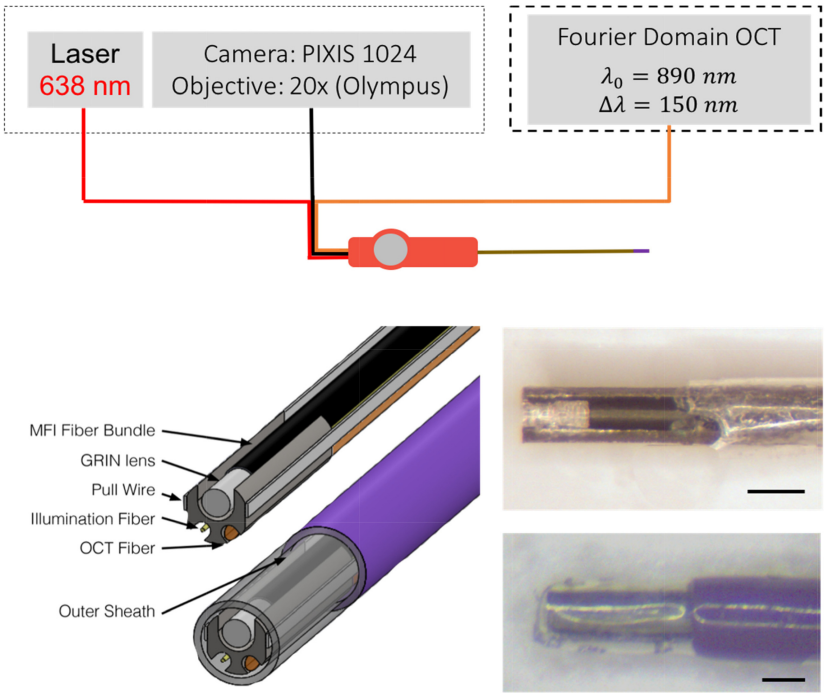

Fig. 1. System overview (top) and distal tip overview (bottom left) showing detailed inner components and the orientation in the sheath. The illumination fiber is shown in red (top) and in gold (bottom left), the OCT fiber in orange, and the fiber bundle in black. In this iteration, we use a single 638nm fiber coupled laser for illumination and image the proximal fiber bundle face onto a PIXIS camera. The OCT probe is incorporated as the sample arm into an existing tabletop OCT system. The distal tip uses a ferrule (grey) to hold the components (fiber bundle, GRIN lens, two pull wires, illumination fiber and OCT fiber). These inner components are within the outer sheath of heat shrink (clear tip) and polymer (purple). Photos of the probe are shown (bottom right) with the heat shrink peeled back (top) to reveal the optics and with the heath shrink and outer sheath in place (bottom). Scale bas are 0.5 mm.

Figure 1 depicts the system overview as well as the optical components and mechanical housing of the distal tip of the falloposcope. The optical components consist of 1) an all-fiber side-viewing 125 μm OCT probe, 2) a tapered 110 μm low-OH illumination fiber, and 3) the imaging system which, in this iteration, is a 3,000 element fiber bundle with 250 μm diameter gradient index of refraction (GRIN) imaging lens. These optical components are connected to and aligned by a distal ferrule. The 3 mm long, 560 μm diameter ferrule has slots cut into it with wire electrical discharge machining (EDM) to accommodate the three optical components. At the proximal end of the endoscope the fibers pass through a handle and are then connected to their respective tabletop systems. The sheath varies in material over its length, distally attaches to the ferrule and proximally to the handle. The steering mechanism consists of two flat wires that traverse the full length of the sheath attached distally to the ferrule and proximally to the articulation controller in the handle. The following sections discuss each of these in detail.

3. Optical components

3.1 Optical coherence tomography

The fallopian tube lining is composed of plica extending into the lumen covered by an epithelium of ciliated columnar cells and secretory cells. This epithelium thickens in serous tubal intraepithelial carcinoma (STIC- the putative precursor to ovarian cancer) to at least 4 – 5 cell layers [2], or approximately 50 μm. With an axial resolution of a few micrometers,

Biomedical Optics EXPRESS

OCT is able to identify this thickening adequately. To achieve a desired high axial resolution, we utilize a super luminescent diode (Superlum, Moscow, Russia) with a center wavelength of 890 nm and a bandwidth of 150 nm, yielding a theoretical axial resolution of 2.3 µm in air. This light source is incorporated into a Spectral Domain OCT table-top system previously described in detail [34]. An all-fiber based OCT sample arm probe with an outer diameter of 125 µm, as first explained in Lorenser, et al. [22], was designed, built, and incorporated into the falloposcope.

For this application, lateral resolution is less important than axial resolution, and a specification of 15 µm lateral resolution is sufficient to locate small STICs and to have a reasonable depth of focus of approximately 1 mm (defined as twice the Rayleigh range). The desired focus was 700 µm outside the falloposcope sheath so that the epithelium was within the depth of focus when the probe was placed in contact with the tissue. We modeled the desired behavior using ray-matrix tracing for Gaussian beams in Matlab (The MathWorks, Natick, Massachusetts) using a method described previously to determine lengths of large core fiber (for beam expansion), GRIN fiber (for focusing), and additional large core fiber (to polish for side firing) [35]. To assemble the probe, we spliced together the components: a 2 meter length of single mode fiber (780HP, Thorlabs, Newton, NJ) with the distal ~3 mm stripped of coating, 325 µm length of multimode fiber (FG105LCA, Thorlabs, Princeton, NJ), 95 µm length of GRIN fiber (GIF625, Thorlabs) and an additional 300 µm length of multimode fiber using a Vytran filament fusion splicer (FS-2000, Vytran). Longer lengths were initially spliced, then after each operation the component was cleaved to length under a stereoscope using a cleaver (FK11, York) modified with a micrometer to enable precise length control before splicing to the next component. The distal face was polished to a 48° angle with respect to fiber diameter using a bare fiber polisher (Radian Fiber Polisher, KrellTech, Morganville, NJ). This angle is sufficient for total internal reflection assuming a fiber-air interface.

At the end of this process, the OCT probe is 125 µm diameter (bare fiber diameter) for a length of 3 to 4 mm while the remainder of the 2 m length is 250 µm diameter with the acrylate coating intact. The ferrule has a 3 mm long groove of diameter 135 µm that aligns and protects the delicate distal 3 mm of the OCT probe. Glue is placed at the proximal 1 mm of the ferrule to hold the OCT probe in place and wicks onto the remaining bare fiber, creating additional support and stress relief. The OCT probe used in this prototype is shown in Fig. 2 left. The OCT probe was incorporated into the 890 nm Spectral Domain OCT system and an image of a roll of cellophane tape (Fig. 2 right) confirms adequate performance of the probe by detecting the approximately 50 µm thick alternating layers of adhesive and cellophane film.

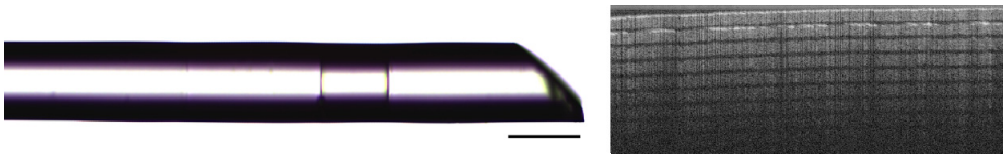

Fig. 2. (Left) Angle polished all-fiber OCT probe with the GRIN fiber segment outlined by its splice marks. The scale bar is 125 µm. (Right) Image of a roll of cellophane tape taken with this probe. The 2.5 mm wide image was collected in a motorized linear pullback collecting 4,000 A-scans/s.

Lateral resolution was determined to be 12.5 µm by measuring the edge response from scanning the probe across lines on a reflective United States Air Force (USAF) bar target. A profile was measured across the edge using ImageJ. This data were then median filtered and fit to a sigmoid of the form:

Biomedical Optics EXPRESS

$$f(x) = a + \frac{b}{1+\exp(-x+c)}$$

where *a, b,* and *c* are fitting coefficients and *x* the data. The line spread function (LSF), the system's response to a line, is approximated by full-width half maximum of the first-order derivative of this curve. Scanning for image acquisition can be obtained by manual rotation and/or pull-back of the entire falloposcope.

3.2 Wide field imaging

Wide field imaging, which may include white light, narrow band, or multispectral fluorescence and reflectance imaging, is the forward viewing modality used to aid navigation and scan for areas of abnormalities. The desired specifications are a working distance of 3-10 mm with a minimum of 60° field of view. Multispectral imaging relies on being able to illuminate the tissue with multiple wavelengths in a concerted manner, building up a stack of reflectance and/or fluorescence emission images. Our illumination system is capable of accommodating white light plus any individual wavelength that can be reasonably coupled into a 100 µm core diameter fiber. In our case potential wavelengths are from UV (250 nm) through visible (638 nm) [36]. The table-top imaging system images the proximal end of the fiber bundle with a 20X Olympus objective onto a CCD camera (PIXIS 1024, Princeton Instruments, Trenton, NJ), through an optional set of emission filters.

3.2.1 Illumination

Due to the size limitations in the falloposcope, there is clearance for only a single illumination fiber. The fiber had to meet the following requirements: 1) have a total outside diameter small enough to fit through the sheath and a cladding diameter small enough to be accommodated in the ferrule, 2) provide illumination for the full 60° field of view of the imaging optics and 3) accommodate UV wavelengths as short as 250 nm and full visible range, to accommodate multiple designs. To achieve this, the maximum outer diameter of the coating was set at 125 µm. The required emission NA, considering the size of the imaged field of view and the offset between the illumination fiber and the imaging fiber, is 0.55. To encompass all potential wavelengths, a low-OH fiber core was required. No off-the-shelf low OH fibers of the required diameter met the required NA, so we modified a low-OH core fiber with 100 µm core and 110 µm cladding diameter (FIP100110125, Polymicro Technologies, Phoenix, AZ) with an inherent NA of 0.22.

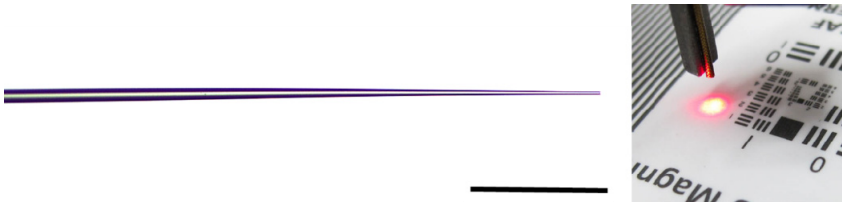

Fig. 3. Characterization of tapered illumination fiber. Image of tapered illumination fiber (left) taken with a microscope. Example output beam (right) of the illumination fiber once incorporated into the falloposcope. The beam is shown on a USAF bar target for contrast. The scale bar is 1 mm.

By tapering the fiber, as shown in Fig. 3, we are able to nearly double the illumination NA, according to:

$$A_i(NA_i)^2 = A_0(NA_0)^2$$

where A is the cross-sectional area of the fiber and the NA is the numerical aperture before and after tapering. The approximately 2 mm long taper was created by first stripping a short

Biomedical Optics EXPRESS

segment of the fiber to remove the polymer coating and then cleaning thoroughly using isopropyl alcohol solution. The stripped segment was then heated up to softening temperature using a butane torch while both fiber ends were pulled apart simultaneously using a motorized stage. The diameter of the fiber in the heated region was reduced gradually as the fiber ends pulled apart. We stopped the pulling process when the fiber diameter reached 10-20 microns at the total pull length of ~1 cm. The tapered fiber was then taken out of the pulling apparatus and cleaved at the thinnest point to form the final device.

Illumination spot diameters were measured at working distances of 3, 5, and 10 mm. The respective illuminated diameters are 4, 5 and 10 mm at the full width half maximum of the line profile, as measured across an image of the beam diameter in ImageJ. This approximately doubles the illumination spot diameter compared to this fiber without a taper (1.3, 2.2 and 4.5 mm, respectively). No visible speckle was noted with tapered fiber illumination. The polyimide coating is strong enough to protect the fiber and smooth enough to fit in the sheath with the other fibers. The ferrule slot is cut to fit this fiber with a 10 μm tolerance and the 3 mm length of the ferrule supports the delicate and bare fiber taper. This fiber drops easily into the slot and is moved to be just set back from the distal end. Glue is placed at the proximal 1 mm of the ferrule to secure the fiber in place and allow for the air interface needed for the tapering effect.

3.2.2 Imaging

To meet the requirements of flexibility and size, we utilize a 3,000 element fiber bundle (FIGH-03-215S, Myriad Fiber) with a 285 μm total diameter and fiber core to core spacing of 3.1 – 3.4 μm. Positive working distance imaging is accomplished by cementing this fiber together with a 0.25 mm diameter GRIN lens (GT-IFRL-025-005-50-NC, Grintech, GmbH, Jena, Germany). The GRIN lens was chosen due to its size and specified paraxial magnification of 23 at a working distance of 5 mm, our nominal desired distance. At these specifications, and with an imaging circle size of 190 μm on the fiber bundle, the system images a 4.4 mm field of view. This design is simple, easy to build, align and affordable for larger scale production, albeit the use of GRIN lens restricts collection of light to wavelengths above approximately 400 nm due to material absorption in the UV. However, UV illumination wavelengths are still useful as they produce visible tissue fluorescence that can be detected. Assembly was performed by hand under a stereomicroscope. This was possible owing to the ferrule's 5 μm tolerance from the wire EDM process and similar diameter between the fiber bundle and GRIN lens. Small drops of glue were placed on the outside of the lens which wicked through the space between the GRIN lens and ferrule. Additional glue at the proximal end of the fiber bundle/ferrule interface held the fiber bundle. No glue was placed between the fiber bundle face and GRIN lens to avoid potential fluorescence, aberrations or artifacts from the glue.

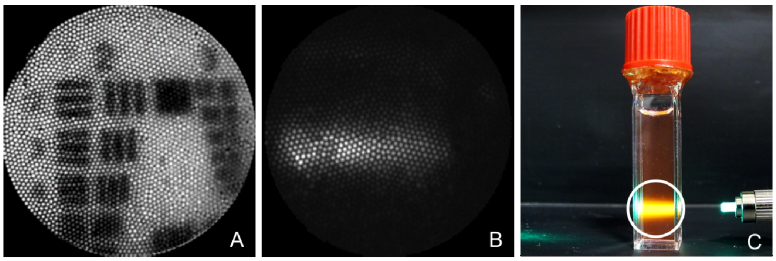

Fig. 4. This figure shows images from the wide field imaging system. A) Image of Group 2 on the USAF resolution target. B) Image taken with the falloposcope of rhodamine fluorescence illuminated by 513 nm excitation and collected through 590 nm narrow band emission filter. C) White light photo showing the target of B. The 1 cm diameter cuvette is filled with rhodamine solution illuminated with 513 nm light. The white circle denotes the field of view of image B.

Biomedical Optics EXPRESS

A USAF bar target was imaged at different working distances to determine the resolution and field of view (FOV). Due to the lack of image space telecentricity, the FOV and associated resolution changes at various working distances. At the target working distance of 5 mm, Group 2 Element 3 is visually resolved, as shown in Fig. 4(A), corresponding to a resolution of 100 µm and a FOV of 4.4 mm. At 3 mm working distance the FOV and resolution are 1.2 mm and 50 µm, respectively, whereas at 10 mm working distance, they are 8.8 mm and 200 µm, respectively. Fluorescence imaging, while not the focus of this paper, is demonstrated by imaging a cuvette of rhodamine solution illuminated with 513 nm light (Fig. 4(C)). A 590 nm narrow band emission filter (Fig. 4(B)) was placed in front of the Pixis camera. The falloposcope tip was placed approximately 1 cm away from the cuvette so that the entire band of fluorescence in the cuvette was in the field of view.

4. Mechanics

The foundation for the mechanics is the custom stainless steel ferrule. All parts were set into place using a medical grade quick set cyanoacrylate (MB297MED, Masterbond, Hackensack, NJ). The cyanoacrylate was chosen over UV curing adhesives or two-part epoxies because its high viscosity of 2,200 – 2,400 cps minimized undesirable wicking and fast curing time (< 60 sec) allowed the components to be fixed in place while maintaining alignment. Two-part epoxies cure too slowly to maintain alignment and UV curing adhesives are inappropriate because the glue is placed between opaque materials, e.g. stainless steel and polymer, and therefore may not cure fully. In addition to the optical components described above, the ferrule is also the attachment point for steering wires. Steering is achieved with the use of two stainless steel flat wires (25 µm x 75µm, Fort Wayne Metal) which are glued to flats on the outside of the ferrule. Gluing minimized the diameter over other common methods of attachment such as a u-bend. The small size of the wires and ferrule makes welding difficult.

The sheath was designed to: 1) be of small enough outer diameter to easily fit through the ~1 mm diameter ostium opening, 2) be of large enough inner diameter to accommodate the ferrule/optics/wire assembly as well as enable threading of the fibers and wires through its 1 m length, 3) be atraumatic and flexible, yet pushable, through most of its length, and 4) accommodate very high flexibility and minimal rigid length at the distal end to allow steering. The overall sheath is 1 m in length: this is to travel the length of the fallopian tube (7 – 15 cm), traverse the hysteroscope (26 to 34 cm), and have additional length for the physician to manipulate the handle comfortably away from the patient.

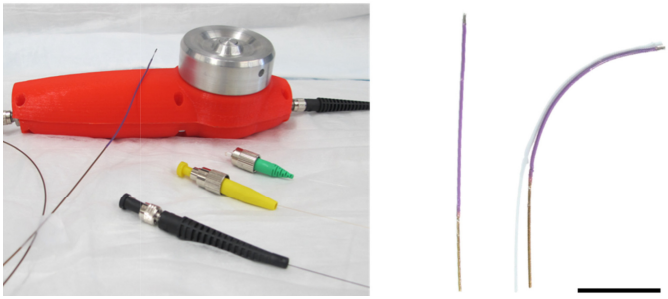

Fig. 5. Overview of the falloposcope prototype. The red handle (left) was 3D printed in PLA to help assess ergonomics while showing proof of concept for connections. The falloposcope exits the left side, the handle is designed to be help upright in one hand, and the three fibers exit the right side where they are connectorized proximally. The distal sheath (right) is shown bending with a pull wire activated and straight in its neutral position. The scale bar is 2.5 cm.

Laser-cut stainless steel hypotubing was initially tested for the sheath due to its well-understood mechanical properties, low cost, biocompatibility, and ability to be sterilized by multiple methods. This design was ultimately rejected due to the high friction both between sheath and fibers/wires, and sheath and tissue, necessitating the use of PTFE liners which

Biomedical Optics EXPRESS

increased diameter and were difficult to push into place. The stainless steel hypotubing was also fragile when laser cut at the wall thicknesses desired. At a 50 μm wall thickness and 0.7 mm outer diameter, the tubing tended to buckle under compressive strain and could fail due to fatigue under repeat bending. The increases in diameter and wall thickness necessary to mitigate these problems were too large to be acceptable for the falloposcope. However, laser-cut stainless steel with PTFE liner and lubricious coating may be an attractive design option for other (larger diameter) applications.

Polymers and multilayered tubing can be made with thinner walls compared to metal while still maintaining the desired pushability. Multilayered tubing can incorporate a PTFE liner, facilitating placement of the pull wires and fibers in assembly. Its strength comes from braided stainless steel wire and biocompatible coating from an outer polyimide layer. The braided tubing effectively transmits torque, meaning that proximal rotation of the sheath handle is transmitted to the distal tip, providing intuitive control. A multilayer braided sheath (142-0015, Vention Medical, Salem, NH) 0.787 mm outer, 0.635 mm inner diameter was used for the majority of the length of the falloposcope.

Pebax nylons come in a variety of Shore D hardness ranges, yielding options for portions of the endoscope where greater flexibility is needed, in our case the steered distal tip. Off-the-shelf Pebax35D tubing (2 Fr sheath, Zeus Medical, Orangeburg, SC) was used for this purpose in the distal 5 cm. This tubing has a 0.66 mm inner diameter and wall thickness of 0.127 mm, for a total outer diameter of 0.914 mm. Custom Pebax tubing maintaining the inner diameter but thinner walls can be used to match the outer diameter of the braided tubing. Polymer to polymer bonding such as Pebax to the multilayer sheath tend not to be amenable to adhesives. Bonding at this site was achieved by heat to the multilayered sheath with plasma treated possible for other attachment methods. At the ferrule, the Pebax was attached using adhesive and thin-walled polyester heat shrink (103-0156, Vention Medical, Salem, NH), which extended to the end of the ferrule, protecting the fibers and allowing transmission of the 890 nm light of the OCT system.

At the proximal end of the falloposcope, a handle was designed that provided ergonomic manipulation of the falloposcope, pass-through and strain relief (using SMA connectors) of fibers, and manipulation of the pull wires. A 90° bend in the falloposcope distal 5 cm Pebax section (the purple material in Fig. 5) was achieved when the pull wires were translated 4 mm. The bending radius was limited by the fibers stiffness, the force applied to the wires as well as the ratio between the length of the rigid ferrule (3 mm) and the length of the Pebax, like any cantilever. The pull wires were tensioned to a pulley in the handle during assembly of this prototype, and the pulley was designed to actuate 90° bend, or 3.4 cm bend radius, with an approximately quarter-turn of the pulley knob. Improved bending of the distal tip could be accomplished by fixing the pull wires in their own guidance channels. The current handle was 3D printed with PLA, and the pulley and knob are machined aluminum. Photographs of the assembled falloposcope are shown in Fig. 5.

5. Results

5.1 Imaging in a tissue model

The falloposcope is designed to traverse the working channel of a hysteroscope. To show proof of concept, we use the working channel and the light from a neonatal intubation fiberscope (11301AB1, Karl Storz, Germany). Figure 6(A) shows our prototype entering the working channel and the inset shows the falloposcope exiting the distal working channel. Finding, docking with and entering the ostium is a known challenge; one that can be eased by using the hysteroscope video system to visualize the uterine wall and falloposcope together on one screen. Once inside the tube, the falloposcope forward viewing channel helps the user navigate down the lumen and the soft tip helps track along the wall without puncturing it.

Biomedical Optics EXPRESS

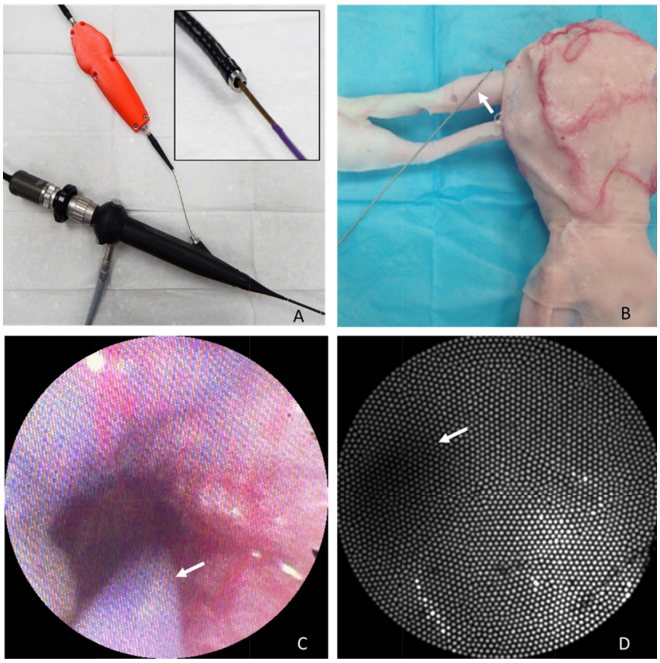

Fig. 6. Testing the falloposcope in a female reproductive tract model. A) The falloposcope passing through the working channel of a bronchoscope. B) The female reproductive tract model is shown with falloposcope (arrow) for scale. C) Frame from the bronchoscope's camera of the falloposcope (arrow) entering the ostium, see Visualization 1. D) View from the falloposcope wide field imaging channel within the fallopian tube, illuminated with 638nm light. The arrow points to the dark section representing the lumen of the tube. The ostium inner diameter in this model is 2.5 mm.

To test the falloposcope mechanics and simulate physician use, we tested it in the University of Arizona Simulation Technology and Education Center (ASTEC) using an artificial tissue model created through a collaborative between Syndaver®Labs and ASTEC, shown in Fig. 6. The model is made of hydrogels that includes embedded red and blue threads to simulate blood vessels. The inner diameter of the ostium on the model is 2.5 mm. Figure 6(B) shows the outside of the model with the falloposcope for scale (the white arrow is pointing to the tip). Figure 6(C) shows a frame from the video channel of the bronchoscope camera, showing the falloposcope entering the ostium (arrow points to the purple Pebax of the sheath). Figure 6(D) is the view from the falloposcope wide field imaging system of the fallopian tube in reflectance mode using 638 nm light for illumination. The walls of the fallopian tube show smooth, fairly uniform reflected light whereas the lumen of the tube is a darker region. Punctate and linear light and dark pixels are artifacts of the fiber bundle.

5.2 Tissue imaging

To test the falloposcope performance on tissue, porcine fallopian tubes were acquired from local slaughterhouses in a manner approved by the University of Arizona's Institutional Animal Care and Use Committee. The fallopian tube was cut open to expose the lumen. To acquire wide field images, the falloposcope was mounted to a jig and placed 5 mm above the lumen surface. Images were acquired at video rate, example shown in Fig. 7(A). To acquire OCT, the falloposcope without the heat shrink was placed on a coverslip pressing the mucosal side of fallopian tube flat. A longitudinal image of 4,000 A-scans/s was acquired using a linear motor. The wide field image shows some contrast in this fairly uniform tissue, which is more apparent in video mode than the still frame shown here. Punctate dark spots are fiber

Biomedical Optics EXPRESS

bundle artifact. The OCT image shows the muscle layer (M) and folding of the interior epithelial surface (E).

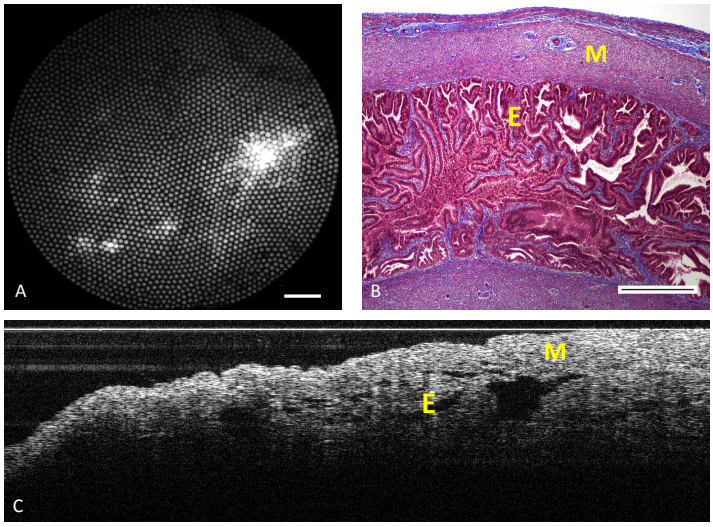

Fig. 7. Imaging porcine fallopian tube. A) Reflectance imaging of the lumen using the falloposcope and 638 nm illumination at 5 mm working distance. Scale bar is 0.5 mm B) Representative histology section (stained with Masson Trichrome) of fallopian tube showing muscle layer (M) and epithelial lumen (E). Scale bar is 0.5 mm. C) A longitudinal OCT scan of the mucosal side of fallopian tube covered with a coverslip. The image was taken with a motorized linear pullback scan of 4,000 A-scans/s over a longitudinal distance of 2 mm.

6. Discussion

We have shown that it is possible to miniaturize and combine side-viewing OCT and forward viewing wide field imaging in a novel sub-millimeter package. Combining the optics with a sheath that is flexible and steerable at this size is a manufacturing challenge which nonetheless is achievable and potentially could be automated. We show that this prototype fits into the biopsy channel of an existing endoscope and can image both tissue models and fallopian tube tissue.

This falloposcope would be used in a similar fashion to commercially available endoscopes. That is, the user would control tip articulation from the handle and feed the falloposcope distal tip forward manually while viewing a monitor displaying the image. Once inside the fallopian tubes, the wide field imaging allows navigation and visualization of the tubal epithelium. The falloposcope is compatible with multispectral imaging, which has been shown to differentiate between normal, benign, and cancerous ovary and fallopian tube tissue [16]. If a region of interest is seen, the falloposcope can be steered to bring that region into the center of the screen and to navigate slightly past. The user would then rotate the handle to place the OCT in contact with the wall, and acquire a 2D pull back or rotational OCT image. The handle could be designed with motorized, automated pull back for OCT imaging.

The side-viewing OCT is not within the field of view of the wide field imaging modality because its tip is set back in the ferrule for improved mechanical stability. However, the OCT beam exits the falloposcope at a known location, therefore it is possible to correlate its output with the wide field image. Initially, this procedure will likely require a skilled physician with an assistant to perform, but could be automated with linear and rotational motors in the proximal handle. Finding, entering and full inspection of both fallopian tubes may take up to an hour of time. A fast acting local anesthetic, lidocaine for example, administered through the hysteroscope would ameliorate fallopian tube spasm and might also be necessary for patient comfort.

Biomedical Optics EXPRESS

While the addition of OCT adds a level of complexity, the basic clinical workflow and procedure time remains the same as for falloposcopy procedures performed in the 1990s. We improve on existing white-light endoscopes of this size, also limited to 3,000 fibers, by creating a platform that is compatible with a broad range of UV and visible illumination wavelengths. This potentially enables multispectral fluorescence imaging and obtaining information on the tissue health from endogenous chromophore concentrations. Taking multiple images at various wavelengths and creating ratiometric combined images could mitigate white-out, a complication common to all reflectance-based tissue imaging.

More work remains to be done to bring this prototype to a stage where it could be tested in the clinic. Most importantly, a cover plate needs to be added to the design to separate the GRIN material from the body. Potential solutions include a fused silica plate, or use of conventional lenses made from biocompatible material. If UV illumination wavelengths are not needed, a dip coat or adhesive potting material can be employed. The use of a dip coat or potting material could also eliminate the need for heat shrink, creating a simple and durable coating. The materials and adhesives in the current distal *in vivo* end were chosen to be compatible for sterilization. Sterilization tests of the complete system should be performed to assess any changes in optical or mechanical performance. It may be feasible to assemble the falloposcope at low enough cost that it could be manufactured in a sterilized environment, creating a disposable device used for one patient. Additional testing needs to be performed on the sheath to assess its ability to navigate the human fallopian tube and ovary as well as to determine its behavior in the collapsed fallopian tube. If necessary, the saline channel on the hysteroscope can be utilized and saline can be flushed through the fallopian tube to gently open it. We are also investigating the use of an everting balloon to guide the falloposcope through the fallopian tube [37].

Funding

Department of Defense (W81XWH-13-1-0131); The National Institutes of Health/ National Institute of Biomedical Imaging and Bioengineering (U54EB015403); Arizona Technology Research Innovation Fund Imaging Fellowship and the Achievement Rewards for College Scientists (ARCS) Phoenix Chapter.